JOURNAL OF ENVIRONMENTAL SCIENCES 94 (2020) 81–88

Available online at www.sciencedirect.com

ScienceDirect

www.elsevier.com/locate/jes

JES JOURNAL OF ENVIRONMENTAL SCIENCES

www.jesc.ac.cn

Effect of potential HONO sources on peroxyacetyl nitrate (PAN) formation in eastern China in winter

Jingwei Zhang[1,2], Yitian Guo[1,2], Yu Qu[1], Yong Chen[1], Ruipeng Yu[3], Chaoyang Xue[2,4], Rui Yang[5], Qiang Zhang[6,7], Xingang Liu[8], Yujing Mu[2,4,9], Jing Wang[3], Can Ye[2,4], Haihan Zhao[3], Qiangqiang Sun[10], Ziwen Wang[11], Junling An[1,2,9,*]

[1] *State Key Laboratory of Atmospheric Boundary Layer Physics and Atmospheric Chemistry (LAPC), Institute of Atmospheric Physics (IAP), Chinese Academy of Sciences, Beijing 100029, China*
[2] *College of Earth Science, University of Chinese Academy of Sciences, Beijing 100049, China*
[3] *College of Resources and Environmental Sciences, China Agricultural University, Beijing 100193, China*
[4] *Research Center for Eco-Environmental Sciences, Chinese Academy of Sciences, Beijing 100085, China*
[5] *Guangzhou Meteorological Observatory, Guangzhou 511430, China*
[6] *Ministry of Education Key Laboratory for Earth System Modeling, Department of Earth System Science, Tsinghua University, Beijing, China*
[7] *Collaborative Innovation Center for Regional Environmental Quality, Beijing, China*
[8] *State Key Laboratory of Water Environment Simulation, School of Environment, Beijing Normal University, Beijing 100875, China*
[9] *Center for Excellence in Urban Atmospheric Environment, Institute of Urban Environment, Chinese Academy of Sciences, Xiamen 361021, China*
[10] *College of Land Science and Technology, China Agricultural University, Beijing 100193, China*
[11] *Qinghai Climate Center, Qinghai Meteorological Bureau, Xining, Qinghai 810001, China*

ARTICLE INFO

Article history:
Received 9 September 2019
Revised 5 March 2020
Accepted 12 March 2020
Available online 4 May 2020

Keywords:
Nitrous acid (HONO)
Peroxyacetyl nitrate (PAN)
WRF-Chem model
Winter haze
RO_x cycles

ABSTRACT

As an important secondary photochemical pollutant, peroxyacetyl nitrate (PAN) has been studied over decades, yet its simulations usually underestimate the corresponding observations, especially in polluted areas. Recent observations in north China found unusually high concentrations of PAN during winter-time heavy haze events, but the current model still cannot reproduce the observations, and researchers speculated that nitrous acid (HONO) played a key role in PAN formation. For the first time we systematically assessed the impact of potential HONO sources on PAN formation mechanisms in eastern China using the Weather Research and Forecasting/Chemistry (WRF-Chem) model in February of 2017. The results showed that the potential HONO sources significantly improved the PAN simulations, remarkably accelerated the RO_x (sum of hydroxyl, hydroperoxyl, and organic peroxy radicals) cycles, and resulted in 80%–150% enhancements of PAN near the ground in the coastal areas of eastern China and 10%–50% enhancements in the areas around 35–40°N within 3 km during a heavy haze period. The direct precursors of PAN were aldehyde and methylglyoxal, and the primary precursors of PAN were alkenes with C > 3, xylenes, propene and toluene. The above results suggest that the potential HONO sources should be considered in regional and global chemical transport models when conducting PAN studies.

Introduction

Peroxyacetyl nitrate (PAN) is one of the most important photochemical pollutants in the atmosphere, and could threaten human health and damage plants (Hanson and Stewart, 1970; Kleindienst, 1994; Yukihiro et al., 2012). PAN is directly formed via the reaction between the peroxyacetyl radical ($CH_3C(O)O_2$, i.e., PA) and NO_2 (R1), and PA is mainly produced via atmospheric oxidation of volatile organic compounds (VOCs) by the hydroxyl radical (OH) (R2). Primary precursors of PA are isoprene, anthropogenic alkenes and aromatics (Grosjean et al., 1993; Liu et al., 2010; Xue et al., 2014), and immediate carbonyl precursors such as aldehyde (CH_3CHO) and methylglyoxal (MGLY, CH_3COCHO) (Fischer et al., 2014; Xue et al., 2014; Zhang et al., 2015). Thermal decomposition (R3) is the main PAN removal process in the troposphere. PAN

* Corresponding author at: State Key Laboratory of Atmospheric Boundary Layer Physics and Atmospheric Chemistry (LAPC), Institute of Atmospheric Physics (IAP), Chinese Academy of Sciences, Beijing 100029, China.
E-mail address: anjl@mail.iap.ac.cn (J. An).

https://doi.org/10.1016/j.jes.2020.03.039
1001-0742/

can act as a reservoir of NO_2 and can be transported to remote areas in winter, and NO_2 can be released via PAN decomposition as air temperature rises and thus could influence O_3 levels in less polluted areas (Singh and Hanst, 1981; Kotchenruther et al., 2001; Jiang et al., 2016; Xu et al., 2018).

$$CH_3C(O)O_2 + NO_2 \rightarrow PAN \quad (R1)$$

$$VOC_s + OH \xrightarrow{O_2} CH_3C(O)O_2 \quad (R2)$$

$$PAN \rightarrow CH_3C(O)O_2 + NO_2 \quad (R3)$$

East Asia, especially China, is one of the major sources of PAN in the global atmosphere, and has attracted considerable attention recently (Lee et al., 2012; Fischer et al., 2014; Zhu et al., 2017). Many PAN observations have been conducted in China in the past decade, in both summertime (Zhang et al., 2009a, 2015; Liu et al., 2010; Xue et al., 2014; Xu et al., 2018) and wintertime (Zhang et al., 2014, 2019a; Liu et al., 2018; Ye et al., 2018; Qiu et al., 2019). The photochemical reactions are stronger in summer than in winter due to the intense solar radiation, and O_3 and PAN usually have a good positive correlation (Zhang et al., 2009a; Liu et al., 2010; Xue et al., 2014; Xu et al., 2018). However, during wintertime, especially in heavy haze periods, weak correlations between PAN and O_3 but strong positive correlation (R^2 >0.8) between PAN and $PM_{2.5}$ were frequently found (Zhang et al., 2014,2019a; Liu et al., 2018; Ye et al., 2018; Qiu et al., 2019), and PAN concentrations during haze periods could be one order of magnitude higher than those on clean days (Ye et al., 2018; Qiu et al., 2019; Zhang et al., 2019a). Liu et al. (2018) and Zhang et al. (2019a) speculated that the photolysis of nitrous acid (HONO) produced OH (R4) during haze periods probably played a crucial role in PAN formation, and that heavy haze promoted HONO formation via NO_2 heterogeneous reactions (R5) on aerosol surfaces (Liu et al., 2018).

$$HONO \xrightarrow{h\nu} NO + OH \quad (R4)$$

$$2NO_2 + H_2O(ads) \rightarrow HONO(g) + HNO_3(ads) \quad (R5)$$

As one of the dominant sources of OH, HONO contributes 20%–80% of the primary OH production (Alicke et al., 2003; Hendrick et al., 2014; Kim et al., 2014; Gligorovski et al., 2015; Tang et al., 2017), and the contribution could be even larger in a winter haze period due to the weak photolysis of O_3 (Hendrick et al., 2014; Liu et al., 2018; Zhang et al., 2019c). Many HONO formation pathways in addition to the gas-phase production of HONO (NO+OH → HONO) have been proposed, including direct emissions from traffic (Kurtenbach et al., 2001), from biomass burning (Rondon and Sanhueza, 1989; Nie et al., 2015; Stockwell et al., 2015) and from soil (Bhattarai, et al., 2019; Wu et al., 2019; Xue et al., 2019), as well as NO_2 heterogeneous reactions on ground/aerosol surfaces (Finlayson-Pitts et al., 2003; Kleffmann and Wiesen, 2005; Ma et al., 2013; Tang et al., 2017) or sea surfaces (Zha et al., 2014; Cui et al., 2019; Wen et al., 2019), and the photolysis of nitric acid/nitrate (Zhou et al., 2001; Laufs and Kleffmann, 2016; Tsai et al., 2018). Recent observations in China confirmed a strong positive correlation between HONO and $PM_{2.5}$ during winter haze periods (Liu et al., 2014; Hou et al., 2016; Zhang et al., 2019d), thus emphasizing the key role of aerosols on HONO formation. Elevated HONO during a winter haze period could in turn enhance atmospheric oxidation capacity, aggravate haze events and might facilitate PAN formation.

Over the last decade, potential HONO sources have been inserted into regional chemical transport models (e.g., the Community Multiscale Air Quality (CMAQ) model and the Weather Research and Forecasting/Chemistry (WRF-Chem) model) to assess the impacts of additional HONO sources on $PM_{2.5}$, sulfate, nitrate, O_3 and secondary organic aerosols (SOA) (Sarwar et al., 2008; Li et al., 2010; Zhang et al., 2019b; Tang et al., 2015), yet the impact of additional HONO sources on PAN formation was rarely discussed except few sensitivity studies without corresponding PAN observations (Elshorbany et al., 2012b; Li et al., 2015). On the other hand, several simulations of PAN were conducted using global chemical transport models (Kasibhatla et al., 1993; Singh et al., 2007; Fischer et al., 2014; Jiang et al., 2016; Huang et al., 2017) but the global models underestimated PAN concentrations in China and Europe (Fischer et al., 2014) and in the Arctic (Huang et al., 2017). Recently, Qiu et al. (2019) conducted a simulation of PAN in Beijing using the WRF-Chem model during a winter haze period in 2017, and found that the CBM-Z mechanism performed better than the RADM2 mechanism due to a faster PAN formation rate, but still underestimated PAN observations by ~40%.

In our previous work, we well reproduced the observed HONO after adding six potential HONO sources (i.e., indoor, biomass burning, traffic, and soil emissions, and heterogeneous reactions on aerosol and ground surfaces) into the WRF-Chem model at urban and rural sites, and evaluated the impacts of the six HONO sources on atmospheric oxidation capacity and SOA (Zhang et al., 2019b, 2019c). In this study, a whole month simulation of PAN in February of 2017 was done twice (with/without the six potential HONO sources) using the updated WRF-Chem model to assess the impact of the potential HONO sources on PAN formation. RO_x (sum of hydroxyl, hydroperoxyl, and organic peroxy radicals) budgets with/without the potential HONO sources were calculated during a typical non-haze day and a heavy haze day, PAN formation pathways and its main precursors were explored during the heavy haze days, and the uncertainties in parameterization of potential HONO sources and NO_x/VOCs emissions on PAN formation were discussed. This study helps to further understand the formation process of PAN in the atmosphere, highlights the significance of the six potential HONO sources on PAN formation, and can be adopted to improve PAN simulations regionally and globally.

1. Materials and methods

1.1. Observed data description

Observed PAN concentrations were obtained from Qiu et al. (2019). Measurements were conducted at an urban site (Baolian (BL, 39.93°N, 116.28°E) in Beijing), and a rural site (Shangdianzi (SDZ, 40.65°N, 117.12°E) located ~100 km northeast of the BL site). Detailed descriptions of observation equipment and the two sites can be found in Qiu et al. (2019). HONO measurements were not available at both sites, thus we used observed HONO data (reported in Zhang et al., 2019c) from another rural site of Wangdu (38.67°N, 115.25°E), a regional representative site in the North China Plain (NCP) located ~160 km southwest of the BL site. The HONO measurements were conducted during a heavy haze period from Nov. 29 to Dec. 3 of 2017, the detailed measurements were provided in Xue et al. (2019), and the corresponding simulation evaluation can be found in our previous work (Zhang et al., 2019c). Surface concentrations of O_3 and NO_2 were taken from http://beijingair.sinaapp.com/, issued by the China Ministry of Ecology and Environment; surface meteorological observations were obtained from the National Climatic Data Center, China Meteorological Administration (Wang et al., 2014), totally 89 O_3/NO_2 observation sites and 300 meteorological observation sites were chosen, and detailed locations of these observation sites are given in Fig. S1.

1.2. Model setup

WRF-Chem model version 3.7.1 was used in this study and the corresponding physical and chemical options are shown in Table 1. Two domains of 82 × 64 and 90 × 108 grid cells were

Table 1. – Physical and chemical options in the WRF-Chem model used in this study.

Options	WRF-Chem
Advection scheme	Runge–Kutta 3rd order
Boundary layer scheme	YSU
Cloud microphysics	Lin et al. (1983)
Cumulus parameterization	New Grell scheme
Land-surface model	Noah
Long-wave radiation	RRTM
Short-wave radiation	Goddard
Surface layer	Revised MM5 Monin–Obukhov scheme
Aerosol option	MOSAIC
Chemistry option	Updated MOZART mechanism
Photolysis scheme	F-TUV

used in this simulation. Domain 1 covered east Asia with a horizontal resolution of 81 km, and domain 2 covered eastern China with a horizontal resolution of 27 km. The anthropogenic emission inventory with a resolution of 0.25° was from Zhang et al. (2009b) and updated to 2016 in this study, including CO, NO_x, VOCs, SO_2, $PM_{2.5}$, PM_{10}, glyoxal and MGLY. NH_3 and biogenic VOCs emissions can be found in Zhang et al. (2019b). Two simulations (base and 6S cases) were conducted in February of 2017 with a spin-up period of 7 days. For the base case, the Model for Simulating Aerosol Interactions and Chemistry (MOSAIC) and the updated mechanism of the Model for Ozone and Related chemical Tracers version 4 (MOZART-4) were used, and only the gas-phase production of HONO was considered (Zhang et al., 2019b). For case 6S, the six potential HONO sources were inserted into the model, and the updated model well reproduced observed summer/winter HONO concentrations in our previous studies (Zhang et al., 2019b, 2019c). In this study, the nighttime uptake coefficient of NO_2 on aerosol surfaces was adjusted to 1×10^{-5} from 5×10^{-6}, and the nighttime yield of HONO from NO_2 reaching the surface was adjusted to 0.25 from 0.20 at night to better simulate nighttime HONO concentrations, while other HONO sources were remained the same as those in Zhang et al. (2019b).

Twelve additional cases shown in Table S3 were added to assess impacts of the uncertainties in the uptake coefficient (γ) of NO_2 heterogeneous reactions on aerosol and ground surfaces on HONO and PAN simulations, impacts of the uncertainties in NO_x/VOCs emissions on PAN simulations, and the impact of the NO_2 heterogeneous reaction on the sea surface on HONO and PAN simulations.

2. Results and discussion

2.1. Comparison of simulations and observations

The simulations of air temperature and relative humidity well followed the corresponding observed diurnal variations at 300 representative sites over eastern China in February of 2017 (Fig. S2), and the simulated wind speed overall reproduced the observed trend but showed some overestimations (Fig. S2) due to the exclusion of the urban canopy (Liu et al., 2017; Chen et al., 2018) and the difficulties in parameterization of the stable boundary layer over heterogeneous surfaces (Fernando and Weil, 2010; Hu et al., 2013). The statistical parameters demonstrated that the simulations of air temperature, relative humidity and wind speed at the 300 sites were comparable with the previous studies as shown in Table S1, and the wind direction bias within 45° was over 60%. Averaged daily variations of O_3 and NO_2 from the 89 representative sites were well simulated, and the six potential HONO sources significantly improved daily O_3 maximum simulations in February (Figs. S3, S4).

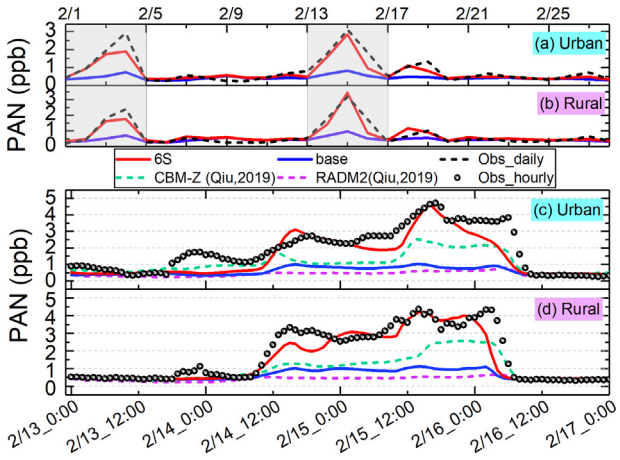

Fig. 1 – Comparison of simulated and observed PAN concentrations at the BL (urban) (a and c) and SDZ (rural) (b and d) sites in February of 2017 (upper panel) and during a heavy haze period of Feb.13–16, 2017 (lower panel). The gray shadows in the upper panel denote the two heavy haze events.

Daily simulated and observed PAN concentrations in February are shown in the upper panel of Fig. 1. The base case performed well during the non-haze periods of Feb. 5–13 and Feb. 20–28, but severely underestimated the observations by 1–2 ppb during the polluted periods of Feb. 1–4 and Feb. 14–16, at both urban (Fig. 1a) and rural sites (Fig. 1b). When the potential HONO sources were inserted into the WRF-Chem model (case 6S), the simulated PAN concentrations were greatly improved (Fig. 1a, b), especially for the two peaks during the polluted periods. The monthly averaged PAN observation was 0.86 (0.73) ppb at the BL (SDZ) site, while the corresponding PAN simulation was 0.75 (0.74) ppb for case 6S and 0.47 (0.44) ppb for base case.

Qiu et al. (2019) compared simulated and observed hourly PAN concentrations at the two sites during Feb. 13–16, the detailed comparison between our simulations and their results is shown in the lower panel of Fig. 1. The CBM-Z mechanism, which had a better simulation than the RADM2 mechanism due to a faster reaction rate of PAN formation (Qiu et al. (2019), still substantially underestimated the PAN observation by ~40% (Fig. 1c, d, Table S2). Our simulation of PAN for the base case was between the two mechanisms (i.e., CBM-Z and RADM2) simulations and underestimated by ~60%, whereas that for case 6S well agreed with the observation at both urban and rural sites, and the underestimation was improved to ~10%–20% (Table S2), indicating the significant role of the potential HONO sources in PAN formation during a winter heavy haze period (Fig. 1c, d, Table S2).

2.2. RO_x budgets at the urban site on both non-haze and heavy haze days

To better understand how HONO affects PAN formation on a non-haze day and a heavy haze day, detailed RO_x budgets at the urban site were computed during daytime (8:00–17:00) on a non-haze day of Feb.13 (Fig. 2a) and a heavy haze day of Feb.15 (Fig. 2b). As expected, most radical production and loss reactions were accelerated on the heavy haze day compared with those on the non-haze day. For the base case, the total production (loss) rate of RO_x (sum of OH, HO_2 and RO_2) was 2.25 (2.25) ppb/h on the non-haze day (Fig. 2b) whereas that was 7.96 (7.96) ppb/h on the heavy haze day (Fig. 2b); for the 6S case, the total production (loss) rate of RO_x was 4.45 (4.45) ppb/hr on the non-haze day and enhanced to 34.49 (34.49) ppb/h on the heavy haze day.

The contribution of HONO photolysis to OH for the base case was 0.04 ppb/hr on the non-haze day (Fig. 2a) and 0.66 ppb/hr on the heavy haze day (Fig. 2b), while HONO formation via the

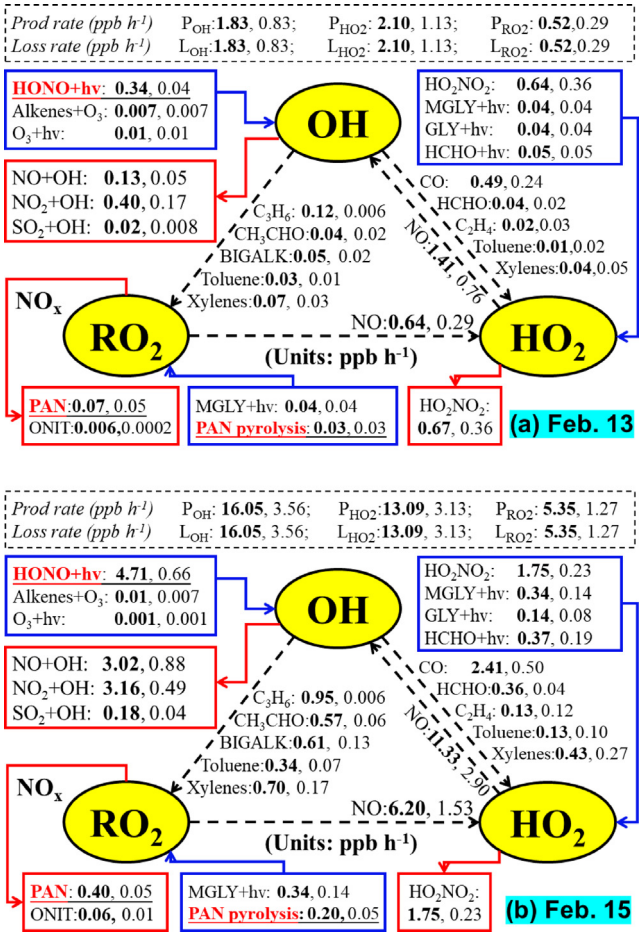

Fig. 2 – RO_x budgets at the BL (urban) site during daytime (08:00–17:00) of the non-haze day (Feb.13, 2017) (a) and the heavy haze day (Feb.15, 2017) (b). Bold numbers: simulations for case 6S; normal numbers: simulations for the base case; blue boxes and lines: main sources of the radicals (arrow in to the three radicals); red boxes and lines: main sinks of the radicals (arrow out to the three radicals); black dashed lines: cycling of the radicals. (For interpretation of the references to color in this figure legend, the reader is referred to the web version of this article.)

reaction of NO+OH was 0.05 ppb/h (Fig. 2a) and 0.88 ppb/hr (Fig. 2b), respectively, so the net contribution of HONO photolysis to OH was −0.01 ppb/hr on the non-haze day and -0.22 ppb/hr on the heavy haze day, meaning that HONO is a sink rather than a source of OH in the base case. When the six potential HONO sources were added (case 6S), the RO_x cycles were substantially accelerated on both non-haze and heavy haze days, e.g., the OH production rate via the photolysis of HONO was enhanced to 0.34/4.71 ppb/hr, 8.5/7.1 times that for the base case on the non-haze/heavy haze day, the OH loss rate via the reaction of NO and OH was enhanced to 0.13/3.02 ppb/hr, 2.6/3.4 times that for the base case on the non-haze/heavy haze day, the net OH production via HONO photolysis was 0.21/1.69 ppb/hr, contributing to > 88% and >99% of the primary OH production on the non-haze day and the heavy haze day, respectively.

Although O_3 photolysis is a main source of OH in summertime, its contribution to OH is small in wintertime, and HONO was the most important primary source of OH at this site (Fig. 2), consistent with previous studies (Elshorbany et al., 2012a; Hendrick et al., 2014; Kim et al., 2014; Tang et al., 2015; Yang et al., 2017;).

The lower left quarter of Fig. 2 shows main production/loss rates of ground PAN. PAN was formed through the reaction of $CH_3CO_3+NO_2$, and decomposed mainly through pyrolysis. For the base case, the net production rate of PAN in the daytime of Feb.13 and Feb.15 was merely 0.02 and 0.00 ppb/h, respectively,

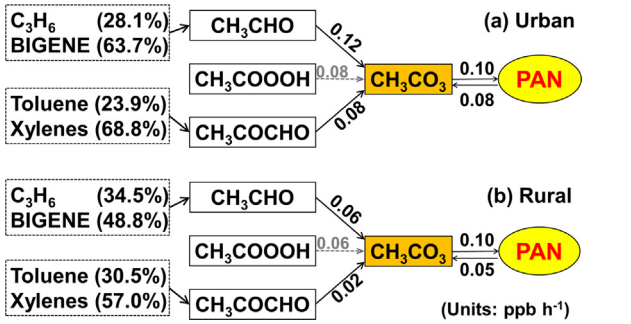

Fig. 3 – Averaged production and loss rates of PAN and CH_3CO_3 (PA), and the major immediate and primary precursors at the BL (urban) (a) and SDZ (rural) (b) sites for case 6S during Feb. 14–16, 2017.

and the simulated PAN concentrations severely underestimated the observations; for the 6S case, the net production rate of PAN in the daytime of Feb.13 and Feb.15 was enhanced to 0.04 and 0.20 ppb/hr, respectively. The net daytime production rate of PAN on the heavy haze day was 5 times that on the non-haze day, corresponding to the slow rise of PAN in the daytime of Feb.13 and the rapid rise of PAN in the daytime of Feb.15, suggesting that the potential HONO sources play a pivotal role in PAN formation during the heavy haze period. This is the main reason for PAN concentrations elevated sharply during winter haze events (Zhang et al., 2014, 2019a; Liu et al., 2018; Ye et al., 2018; Qiu et al., 2019).

2.3. Main PAN precursors at both urban and rural sites

Fig. 3 shows the averaged production and loss rates of PAN and its primary and immediate precursors at both urban and rural sites during Feb.14–16. Clearly, CH_3CHO, peroxyacetic acid (CH_3COOOH), and MGLY were the three most important VOCs for CH_3CO_3 (PA) formation, consistent with previous studies (Fischer et al., 2014; Xue et al., 2014; Zhang et al., 2015) except for CH_3COOOH, which followed a radical cycling pathway of PA. Further analysis of the primary precursors showed that CH_3CHO was mainly formed from atmospheric oxidation of alkenes with C > 3 (BIGENE) and propene (C_3H_6), and MGLY was mainly produced through atmospheric oxidation of xylenes and toluene. At the urban site, the contribution of CH_3CHO to PA (0.12 ppb/hr) was 1.5 times that of MGLY (0.08 ppb/hr), and the contribution of the four primary precursors to PA formation were ~38.2% (63.7% × 0.12/0.20) for BIGENE, ~27.5% for xylenes, ~16.9% for C_3H_6 and ~9.6% for toluene. At the rural site the contribution of CH_3CHO to PA (0.06 ppb/hr) was 3 times that of MGLY (0.02 ppb/h), and the relative contributions of the four primary precursors to PA formation were ~36.6% for BIGENE, ~25.9% for C_3H_6, ~14.3% for xylenes and ~7.6% for toluene. Although isoprene and terpenes were the largest sources of CH_3CHO on a global scale (Fischer et al., 2014), the emissions of these biological VOCs were very small in NCP in winter, indicating anthropogenic VOCs dominated in the studied period. Reactive aromatics were shown to be more important at the urban site (~37%) than at the rural site (~22%), and these results were lower than those of Liu et al. (2010), who estimated that aromatics were the dominant PAN sources (55–75%) using a one-dimensional chemical transport model, the discrepancy between Liu et al. (2010) and our current study could mainly be caused by different adpoted emission inventories.

2.4. Impacts of potential HONO sources on PAN spatial distributions

Fig. 4 presents averaged PAN concentrations for case 6S and the corresponding percentage enhancement of PAN due to the six potential HONO sources in eastern China in February and during Feb.14–16. Higher PAN concentrations (1–2 ppb) were located in

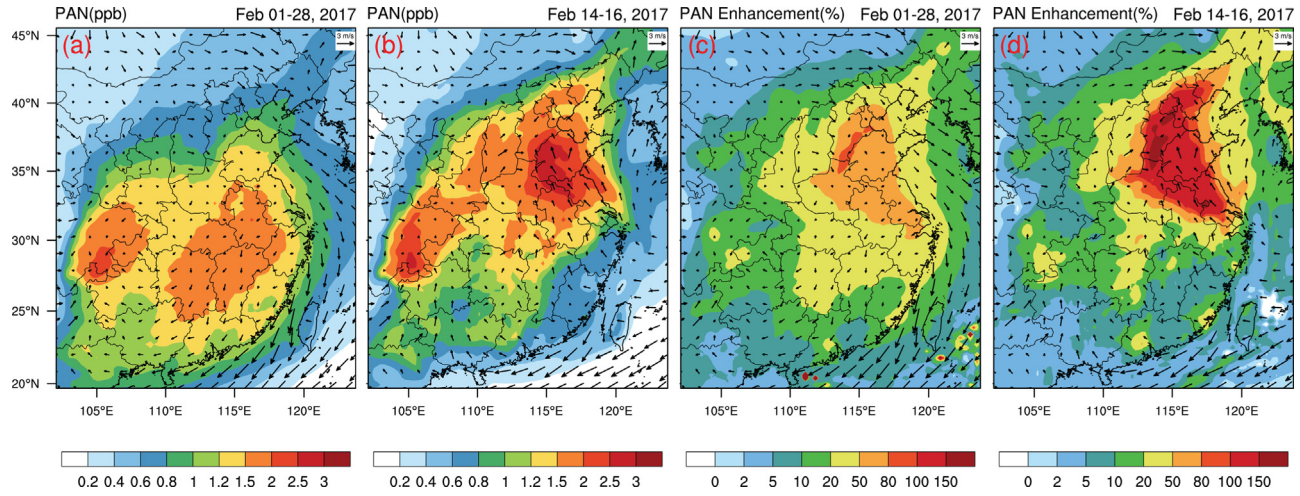

Fig. 4 – Averaged PAN concentrations for case 6S and the corresponding percentage enhancement of PAN due to the six potential HONO sources in eastern China in February and during Feb.14–16, 2017.

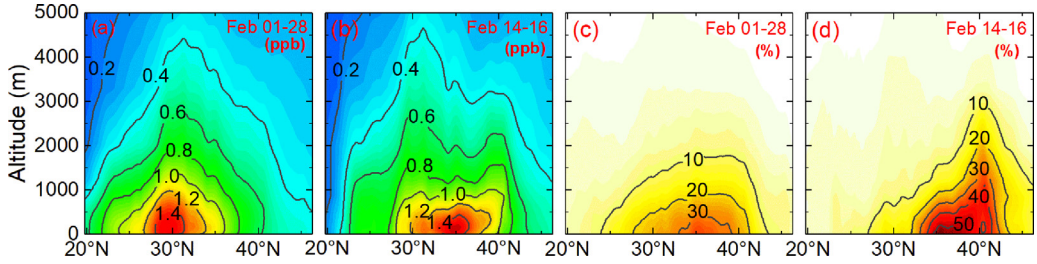

Fig. 5 – Zonal-mean PAN concentrations for case 6S and the corresponding percentage enhancement of PAN due to the six potential HONO sources in eastern China in February and during Feb.14–16, 2017.

southern China (< 35°N) in February, with the largest concentration of 2 ppb in the Sichuan Basin (Fig. 4a). Duing the heavy haze period (Feb.14–16), an anticyclone in the East China Sea led to the pollutants being transported from southeast China to NCP (Fig. 4b, d), and the convergence of the southerly wind caused by the anticylone and the northwestern wind from Siberia and Mongolian resulted in the PAN accumulation (2.5 ppb) in Shandong, southern Hebei, northern Henan, and nothern Anhui. The six potential HONO sources produced a PAN concentration enhancement of 10–80% in most studied areas, with an enhancement of 50–80% being located in the coastal areas of eastern China in February (Fig. 4c), and led to an enhancement of 80–150% in almost the same coastal areas during the heavy haze period (Fig. 4d).

Fig. 5 shows zonal-mean PAN concentrations for case 6S and the corresponding percentage enhancement of PAN due to the six potential HONO sources in eastern China in February and during Feb. 14–16. The largest zonal-mean PAN concentration reached over 1.4 ppb around 30°N within 500 m above the ground, decreasing from 1.2 ppb at 1 km to 0.4 ppb at 4.0 km above the ground (Fig. 5a). Notably, elevated PAN concentrations were transported northward to the areas around 35–40°N under the influence of the anticyclone during the heavy haze period (Fig. 5b, d). The six potential HONO sources led to an enhancement of 10–30% in the areas around 30–40°N within 2 km above the ground in February (Fig. 5c) and that of 10–50% around 35–40°N within 3 km above the ground during the heavy haze period (Fig. 5d).

2.5. Discussion

2.5.1. Impacts of the uncertainty in γ on HONO and PAN simulations

In our previous study, we found that the two heterogeneous reactions on aerosol and ground surfaces were the main HONO sources during daytime, and could significantly affect atmospheric oxidation capacity (Zhang et al., 2019c), and simulations for cases 6S_low and 6S_up were performed to explore the uncertainty in γ on HONO or PAN simulations (Table S3). The γ impact on HONO concentrations at the Wangdu site is shown in Fig. 6. A 50% increase or decrease in γ led to a HONO variation of 0.1–1.5 ppb, large in nighttime and very small in daytime, but did not change the HONO diurnal patterns. At the BL and SDZ sites, A 50% increase or decrease in γ produced a variation of −1.14–1.02 ppb in PAN concentrations with the largest variation in the heavy haze event (Fig. S5; Table S4), suggesting that accurate values of γ are needed, especially for PAN simulations during haze events.

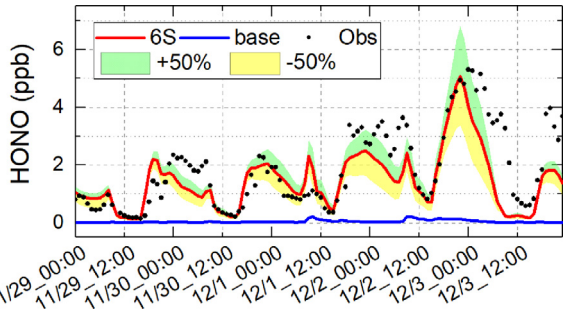

Fig. 6 – Comparison of simulated and observed HONO concentrations at the Wangdu site during Nov.29–Dec. 3 of 2017 (± 50%: changes in the uptake coefficient of NO_2).

2.5.2. Impacts of the uncertainties in NO_x/VOCs emissions on PAN simulations

Both NO_x and VOCs concentrations could affect PAN formation, and eight cases (case A, B, C, D, E, F, G, H) were used to discuss the impact of the uncertainty in the NO_x/VOCs emissions on PAN

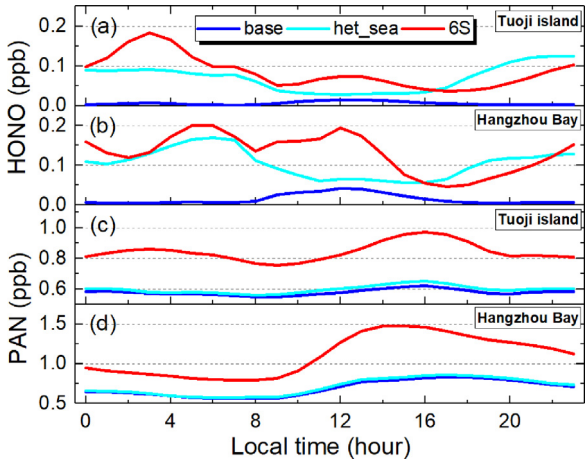

Fig. 7 – Simulated diurnal HONO and PAN concentrations at the Tuji island and the Hangzhou Bay for the base and het_sea cases during February of 2017.

simulations on the basis of case 6S (Table S5). Case I was used to discuss the impact of a 50% increase in VOCs emissions on PAN simulations on the basis of the base case (Table S5).

A 50% increase or decrease in the emissions of NO_x or VOCs produced much larger PAN variations on the heavy haze day than on the non-haze day (Fig. S5, Table S5), and PAN concentrations were more sensitive to VOCs rather than NO_x. Increasing 50% VOCs emissions remarkably enhanced PAN concentrations, while increasing 50% NO_x emissions decreased PAN concentrations with less efficiency (Fig. S5, Table S5). The simulated PAN for case I almost reached that for case 6S even without the six potential HONO soruces. Simulations for cases A–I suggested that accurate emissions of NO_x and VOCs are needed, especially for the emissions of VOCs.

2.5.3. Impact of NO_2 heterogeneous reaction on the sea surface on HONO and PAN simulations

Recently, Cui et al. (2019) and Wen et al. (2019) proposed that the NO_2 heterogeneous reaction on the sea surface was an important HONO source in the Hangzhou Bay (121.75°E, 30.44°N) and Tuoji island (120.74°E, 38.19°N), respectively, both located in the coastal areas of China, and the reported NO_2 to HONO convertion rate ranged from 0.006 to 0.036 hr^{-1} (Zha et al., 2014; Cui et al., 2019; Wen et al., 2019). To evaluate the impact of this newly proposed source on HONO and PAN formation, case het_sea was added with the maximum rate of 0.036 hr^{-1}. Fig. 7 shows the diurnal HONO and PAN simulations for the three cases (base, het_sea and 6S) at the above two sites in February of 2017. After considering the NO_2 heterogeneous reaction on the sea surface, HONO concentrations at the two sites were enhanced by ~0.10 ppb during nighttime and ~0.02–0.05 ppb during daytime (Fig. 7), while PAN concentrations were merely enhanced by 0.01 ppb (nighttime) to 0.03 ppb (daytime), much smaller than the enhancement of 6S case (Fig. 7), suggesting that the impact of the NO_2 heterogeneous reaction on the sea surface on PAN formation is small compared with the other HONO sources (Fig. 4a, c, Fig. 7). Fig. S6 presents the monthly averaged HONO enhancements near the ground due to the NO_2 heterogeneous reaction on the sea surface in eastern China. A HONO enhancement of 0.05–0.20 ppb was found in the coastal regions of china, with the maximum enhancement of 0.20–0.30 ppb along the Bohai Bay, while the HONO enhancement was lower than 0.05 ppb over the ocean.

3. Conclusions

This research made the first attempt to systematically study the impact of six potential HONO sources on PAN formation in eastern China in February of 2017. The observed PAN concentrations were low (0.3–0.5 ppb) on none-haze days and elevated by one magnitude (3–4 ppb) on severe haze days, the CBM-Z, RACM2 and MOZART-4 default mechanisms performed well on clean days but severely underestimated PAN concnetrations by 40–80% on heavy-haze days; the six potential HONO sources, which have been coupled into the WRF-Chem model, signifiantly improved PAN simulations, with the underestimation reducing to 10%–20%. The six potential HONO sources substantially accelerated the RO_x cycles in both non-haze and heavy haze periods, especially in heavy haze periods, and enhanced the net production rate of PAN on a heavy haze day (0.20 ppb/hr) 5 times that on a non-haze day (0.04 ppb/hr). The six potential HONO sources are the key factors to produce unusually high PAN concentrations in wintertime heavy haze periods, and the six potential HONO sources should be taken into account in regional and global chemical transport models to further study PAN formation pathways or mechanisms.

Author contributions

Jingwei Zhang and Junling An designed the research, conducted the simulations and wrote the paper. Yitian Guo, Chaoyang Xue and Can Ye helped to collect PAN and HONO observations. Yu Qu and Yong Chen helped to improve the source code of WRF-Chem model for the detailed production/loss budgets. Ruipeng Yu, Haihan Zhao and Qiangqiang Sun discussed the PAN impact on vegetation growth and agricultural production. Rui Yang and Ziwen Wang helped to collect meteorological observations. Qiang Zhang provided the updated MEIC inventory for this study. Xingang Liu, Yujing Mu and Jing Wang reviewed the paper.

Acknowledgment

This work was partially supported by the National Key Research and Development Program of China (No. 2017YFC0209801), the National Natural Science Foundation of China (Nos. 91544221, 41575124) and the National Research Program for Key Issues in Air Pollution Control (Nos. DQGG0102, DQGG0103).

Supplementary materials

Supplementary material associated with this article can be found, in the online version, at doi:10.1016/j.jes.2020.03.039.

References

Alicke, B., Geyer, A., Hofzumahaus, A., Holland, F., Konrad, S., Patz, H.W., et al., 2003. OH formation by HONO photolysis during the BERLIOZ experiment. J. Geophys. Res. Atmos. 108. doi:10.1029/2001JD000579.

Bhattarai, H.R., Liimatainen, M., Nykänen, H., Kivimäenpää, M., Martikainen, P.J., Maljanen, M., 2019. Germinating wheat promotes the emission of atmospherically significant nitrous acid (HONO) gas from soils. Soil. Biol. Biochem. 136, 107518.

Chen, L., Zhang, M., Zhu, J., Wang, Y., Skorokhod, A., 2018. Modeling impacts of urbanization and urban heat island mitigation on boundary layer meteorology and air quality in Beijing under different weather conditions. J. Geophys. Res. Atmos. 123, 4323–4344. doi:10.1002/2017JD027501.

Cui, L., Li, R., Fu, H., Li, Q., Zhang, L., George, C., et al., 2019. . Formation features of nitrous acid in the offshore area of the East China Sea. Sci. Total Environ. 682, 138–150.

Elshorbany, Y.F., Kleffmann, J., Hofzumahaus, A., Kurtenbach, R., Wiesen, P., Brauers, T., et al., 2012a. HO_x budgets during HO_xComp: A case study of HOx chemistry under NO_x-limited conditions. J. Geophys. Res. Atmos. 117, D03307. doi:10.1029/2011JD017008.

Elshorbany, Y.F., Steil, B., Bruhl, C., Lelieveld, J., 2012b. Impact of HONO on global atmospheric chemistry calculated with an empirical parameterization in the EMAC model. Atmos. Chem. Phys. 12, 9977–10000.

Fernando, H.J.S., Weil, J.C., 2010. Whither the stable boundary layer? AMS 91, 1475–1484. doi:10.1175/2010BAMS2770.1.

Finlayson-Pitts, B.J., Wingen, L.M., Sumner, A.L., Syomin, D., Ramazan, K.A., 2003. The heterogeneous hydrolysis of NO_2 in laboratory systems and in outdoor and indoor atmospheres: an integrated mechanism. Phys. Chem. Chem. Phys. 5, 223–242.

Fischer, E.V., Jacob, D.J., Yantosca, R.M., Sulprizio, M.P., Millet, D.B., Mao, J., et al., 2014. Atmospheric peroxyacetyl nitrate (PAN): a global budget and source attribution. Atmos. Chem. Phys. 14, 2679–2698.
Gligorovski, S., Strekowski, R., Barbati, S., Vione, D., 2015. Environmental implications of hydroxyl radicals (•OH). Chem. Rev. 115, 13051–13092.
Grosjean, D., Williams, E.L., Grosjean, E., 1993. Atmospheric chemistry of isoprene and of its carbonyl products. Environ. Sci. Technol. 27, 830–840.
Hanson, G.P., Stewart, W.S., 1970. Photochemical oxidants: effect on starch hydrolysis in leaves. Science 168, 1223–1224.
Hendrick, F., Müller, J.F., Clémer, K., Wang, P., De Mazière, M., Fayt, C., et al., 2014. Four years of ground-based MAX-DOAS observations of HONO and NO_2 in the Beijing area. Atmos. Chem. Phys. 14, 765–781.
Hou, S.Q., Tong, S.R., Ge, M.F., An, J.L., 2016. Comparison of atmospheric nitrous acid during severe haze and clean periods in Beijing. China. Atmos. Environ. 124, 199–206.
Hu, X.M., Klein, P.M., Xue, M., 2013. 'Evaluation of the updated YSU planetary boundary layer scheme within WRF for wind resource and air quality assessments'. J. Geophys. Res. Atmos. 118, 10490–10505. doi:10.1002/jgrd.50823.
Huang, Y.X., Wu, S.L., Kramer, L.J., Helmig, D., Honrath, R.E., 2017. Surface ozone and its precursors at Summit, Greenland: comparison between observations and model simulations. Atmos. Chem. Phys. 17, 14661–14674.
Jiang, Z., Worden, J.R., Payne, V.H., Zhu, L.Y., Fischer, E., Walker, T., et al., 2016. Ozone export from East Asia: the role of PAN. J. Geophys. Res. Atmos. 121, 6555–6563. doi:10.1002/2016JD024952.
Kasibhatla, P.S., Levy II, H., Moxim, W.J., 1993. Global NO_x, HNO_3, PAN, and NO_y distributions from fossil fuel combustion emissions: a model study. J. Geophys. Res. Atmos. 98, 7165–7180.
Kim, S., VandenBoer, T.C., Young, C.J., Riedel, T.P., Thornton, J.A., Swarthout, B., et al., 2014. . The primary and recycling sources of OH during the NACHTT-2011 campaign: HONO as an important OH primary source in the wintertime. J. Geophys. Res. Atmos. 119, 6886–6896. doi:10.1002/2013JD019784.
Kleffmann, J., Wiesen, P., 2005. Heterogeneous conversion of NO_2 and NO on HNO_3 treated soot surfaces: atmospheric implications. Atmos. Chem. Phys. 5, 77–83.
Kleindienst, T.E., 1994. Recent developments in the chemistry and biology of peroxyacetyl nitrate. Res. Chem. Interm. 20, 335–384.
Kotchenruther, R.A., Jaffe, D.A., Jaegle, L., 2001. Ozone photochemistry and the role of peroxyacetyl nitrate in the springtime northeastern Pacific troposphere: results from the photochemical ozone budget of the Eastern North Pacific Atmosphere (PHOBEA) campaign. J. Geophys. Res. Atmos. 106, 28731–28742.
Kurtenbach, R., Becker, K.H., Gomes, J.A.G., Kleffmann, J., Lorzer, J.C., Spittler, M., et al., 2001. Investigations of emissions and heterogeneous formation of HONO in a road traffic tunnel. Atmos. Environ. 35, 3385–3394.
Laufs, S., Kleffmann, J., 2016. Investigations on HONO formation from photolysis of adsorbed HNO_3 on quartz glass surfaces. Phys. Chem. Chem. Phys. 18, 9616–9625.
Lee, G., Choi, H.S., Lee, T., Choi, J., Jin, S.P., Ahn, J.Y., 2012. Variations of regional background peroxyacetyl nitrate in marine boundary layer over Baengyeong Island, South Korea. Atmos. Environ. 61, 533–541.
Li, G., Lei, W., Zavala, M., Volkamer, R., Dusanter, S., Stevens, P., Molina, L.T., 2010. Impacts of HONO sources on the photochemistry in Mexico City during the MCMA-2006/MILAGO campaign. Atmos. Chem. Phys. 10, 6551–6567.
Li, Y., An, J.L., Kajino, M.Z., Li, J., Qu, Y., 2015. Impacts of additional HONO Sources on concentrations and deposition of NOy in the Beijing-Tianjin-Hebei Region of China. SOLA 11, 36–42.
Lin, Y., Farley, R., Orville, H., 1983. Bulk parameterization of the snow field in a cloud model. J. Appl. Meteorol. 22, 1065–1092.
Liu, L., Wang, X., Chen, J., Xue, L., Wang, W., Wen, L., et al., 2018. Understanding unusually high levels of peroxyacetyl nitrate (PAN) in winter in Urban Jinan, China. J. Environ. Sci. 71, 249–260.
Liu, R., Han, Z., Wu, J., Hu, Y., Li, J., 2017. The impacts of urban surface characteristics on radiation balance and meteorological variables in the boundary layer around Beijing in summertime. Atmos. Res. 197, 167–176. doi:10.1016/j.atmosres.2017.07.006.
Liu, Z., Wang, Y., Costabile, F., Amoroso, A., Zhao, C., Huey, L.G., et al., 2014. Evidence of aerosols as a media for rapid daytime HONO production over China. Environ. Sci. Technol. 48, 14386–14391.
Liu, Z., Wang, Y., Gu, D., Zhao, C., Huey, L.G., Stickel, R., et al., 2010. Evidence of reactive aromatics as a major source of peroxy acetyl nitrate over China. Environ. Sci. Technol. 44, 7017–7022.
Ma, J., Liu, Y., Han, C., Ma, Q., Liu, C., He, H., 2013. Review of heterogeneous photochemical reactions of NO_y on aerosol – a possible daytime source of nitrous acid (HONO) in the atmosphere. J. Environ. Sci. 25, 326–334.
Nie, W., Ding, A.J., Xie, Y.N., Xu, Z., Mao, H., Kerminen, V.M., et al., 2015. . Influence of biomass burning plumes on HONO chemistry in eastern China. Atmos. Chem. Phys. 15, 1147–1159.
Qiu, Y.L., Ma, Z.Q., Li, K., 2019. A modeling study of the peroxyacetyl nitrate (PAN) during a wintertime haze event in Beijing. China. Sci. Total. Environ. 650, 1944–1953.
Rondon, A., Sanhueza, E., 1989. High HONO atmospheric concentrations during vegetation burning in the tropical savannah. Tellus Ser. B – Chem. Phys. Meteorol. 41, 474–477.
Sarwar, G., Roselle, S.J., Mathur, R., Appel, W., Dennis, R.L., Vogel, B., 2008. A comparison of CMAQ HONO predictions with observations from the northeast oxidant and particle study. Atmos. Environ. 42, 5760–5770.
Singh, H.B., Hanst, P.L., 1981. Peroxyacetyl nitrate (Pan) in the unpolluted atmosphere – an important reservoir for nitrogen-oxides. Geophy. Res. Lett. 8, 941–944.
Singh, H.B., Salas, L., Herlth, D., Kolyer, R., Czech, E., Avery, M., et al., 2007. . Reactive nitrogen distribution and partitioning in the North American troposphere and lowermost stratosphere. J. Geophys. Res. 112. doi:10.1029/2006JD007664.
Stockwell, C.E., Veres, P.R., Williams, J., Yokelson, R.J., 2015. Characterization of biomass burning emissions from cooking fires, peat, crop residue, and other fuels with high-resolution proton-transfer-reaction time-of-flight mass spectrometry. Atmos. Chem. Phys. 15, 845–865.
Tang, M.J., Huang, X., Lu, K.D., Ge, M.F., Li, Y.J., Cheng, P., et al., 2017. Heterogeneous reactions of mineral dust aerosol: implications for tropospheric oxidation capacity. Atmos. Chem. Phys. 17, 11727–11777.
Tang, Y., An, J., Wang, F., Li, Y., Qu, Y., Chen, Y., et al., 2015. Impacts of an unknown daytime HONO source on the mixing ratio and budget of HONO, and hydroxyl, hydroperoxyl, and organic peroxy radicals, in the coastal regions of China. Atmos. Chem. Phys. 15, 9381–9398.
Tsai, C., Spolaor, M., Colosimo, S.F., Pikelnaya, O., Cheung, R., Williams, E., et al., 2018. Nitrous acid formation in a snow-free wintertime polluted rural area. Atmos. Chem. Phys. 18, 1977–1996.
Wang, F., An, J.L., Li, Y., Tang, Y.J., Lin, J., Qu, Y., et al., 2014. Impacts of uncertainty in AVOC emissions on the summer ROx budget and ozone production rate in the three most rapidly-developing economic growth regions of China. Adv. Atmos. Sci. 31, 1331–1342.
Wen, L., Chen, T., Zheng, P., Wu, L., Wang, X., Mellouki, A., et al., 2019. Nitrous acid in marine boundary layer over eastern Bohai Sea, China: characteristics, sources, and implications. Sci. Total Environ. 670, 282–291.
Wu, D., Horn, M.A., Behrendt, T., Muller, S., Li, J., Cole, J.A., et al., 2019. Soil HONO emissions at high moisture content are driven by microbial nitrate reduction to nitrite: tackling the HONO puzzle. ISME J. 13, 1688–1699.
Xu, X.B., Zhang, H.L., Lin, W.L., Wang, Y., Xu, W.Y., Jia, S.H., 2018. First simultaneous measurements of peroxyacetyl nitrate (PAN) and ozone at Nam Co in the central Tibetan Plateau: impacts from the PBL evolution and transport processes. Atmos. Chem. Phys. 18, 5199–5217.
Xue, C., Ye, C., Ma, Z., Liu, P., Zhang, Y., Zhang, C., et al., 2019. Development of stripping coil-ion chromatograph method and intercomparison with CEAS and LOPAP to measure atmospheric HONO. Sci. Total. Environ. 646, 187–195.
Xue, L.K., Wang, T., Wang, X.F., Blake, D.R., Gao, J., Nie, W., et al., 2014. On the use of an explicit chemical mechanism to dissect peroxy acetyl nitrate formation. Environ. Pollut. 195, 39–47.
Yang, W.D., Cheng, P., Tian, Z.L., Zhang, M.M., Wang, B.G., 2017. Study on HONO pollution characteristics and daytime unknown sources during summer and autumn in Guangzhou, China. China Environ. Sci. 37, 2029–2039.
Ye, C., Liu, P., Ma, Z., Xue, C., Zhang, C., Zhang, Y., et al., 2018. High H_2O_2 concentrations observed during haze periods in wintertime of Beijing: importance of H_2O_2-oxidation in sulfate formation. Environ. Sci. Technol. Lett. 8, 757–763.
Yukihiro, M., Hiramatsu, T., Bouteau, F., Kadono, T., Kawano, T., 2012. Peroxyacetyl nitrate-induced oxidative and calcium signaling events leading to cell death in ozone-sensitive tobacco cell-line. Plant. Signal. Behav. 7, 113–120.
Zha, Q., Xue, L., Wang, T., Xu, Z., Yeung, C., Louie, P.K.K., 2014. . Large conversion rates of NO2 to HNO_2 observed in air masses from the South China Sea: evidence of strong production at sea surface? Geophys. Res. Lett. 41, 7710–7715.
Zhang, B., Zhao, X., Zhang, J., 2019a. Characteristics of peroxyacetyl nitrate pollution during a 2015 winter haze episode in Beijing. Environ. Pollut. 244, 379–387.
Zhang, G., Mu, Y., Zhou, L., Zhang, C., Zhang, Y., Liu, J., et al., 2015. Summertime distributions of peroxyacetyl nitrate (PAN) and peroxypropionyl nitrate (PPN) in Beijing: understanding the sources and major sink of PAN. Atmos. Environ. 103, 289–296.
Zhang, H., Xu, X., Lin, W., Wang, Y., 2014. Wintertime peroxyacetyl nitrate (PAN) in the megacity Beijing: role of photochemical and meteorological processes. J. Environ. Sci. 26, 83–96.
Zhang, J., An, J., Qu, Y., Liu, X., Chen, Y., 2019b. Impacts of potential HONO sources on the concentrations of oxidants and secondary organic aerosols in the Beijing-Tianjin-Hebei region of China. Sci. Total. Environ. 647, 836–852.
Zhang, J., Chen, J., Xue, C., Chen, H., Zhang, Q., Liu, X., et al., 2019c. Impacts of six potential HONO sources on HO_x budgets and SOA formation during a wintertime heavy haze period in the North China Plain. Sci. Total. Environ. 681, 110–123.
Zhang, J.M., Wang, T., Ding, A.J., Zhou, X.H., Xue, L.K., Poon, C.N., et al., 2009. Continuous measurement of peroxyacetyl nitrate (PAN) in suburban and remote areas of western China. Atmos. Environ. 43, 228–237.
Zhang, Q., Streets, D.G., Carmichael, G.R., He, K.B., Huo, H., Kannari, A., et al., 2009b. Asian emissions in 2006 for the NASA INTEX-B mission. Atmos. Chem. Phys. 9, 5131–5153.
Zhang, W.Q., Tong, S.R., Ge, M.F., An, J.L., Shi, Z.B., Hou, S.Q., et al., 2019d. Variations and sources of nitrous acid (HONO) during a severe pollution episode in Beijing in winter 2016. Sci. Total. Environ. 648, 253–262.
Zhou, X.L., Beine, H.J., Honrath, R.E., Fuentes, J.D., Simpson, W., Shepson, P.B., et al., 2001. Snowpack photochemical production of HONO: a major source of OH in the Arctic boundary layer in springtime. Geophy. Res. Lett. 28, 4087–4090.
Zhu, L.Y., Payne, V.H., Walker, T.W., Worden, J.R., Jiang, Z., Kulawik, S.S., et al., 2017. PAN in the eastern Pacific free troposphere: A satellite view of the sources, seasonality, interannual variability, and timeline for trend detection. J. Geophys. Res. Atmos. 122, 3614–3629.